PHYSICAL REVIEW B VOLUME 25, NUMBER 5 1 MARCH 1982

Magnetic-field study of the energy levels and nonradiative transitions in MgO:Cr^{3+}

M. Ferrari, M. Montagna, O. Pilla, S. Santucci, and G. Viliani
Dipartimento di Fisica, Università di Trento, 38050 Povo, Trento, Italy
and Gruppo Nazionale di Struttura della Materia del Consiglio Nazionale delle Ricerche, Trento, Italy
(Received 25 June 1981)

Excitation spectra of cubic centers in MgO:Cr under magnetic field are reported. The electric and magnetic dipole contributions have been separated. The $^4A_2$-$^4T_2$ zero-phonon line has been studied in detail in order to deduce the energies and shapes of its spin-orbit components. From the analysis of our data, it appears that the effect of interlevel nonradiative transitions in determining widths and shifts of the levels is unusually large.

I. INTRODUCTION

The isoelectronic impurity ions V^{2+} and Cr^{3+} in MgO show anomalous zero-phonon lines (ZPL) for the transition from the ground $^4A_2$ to the excited $^4T_2(\Gamma_6+\Gamma_7+2\Gamma_8)$ state.[1,2] In fact, the expected spin-orbit quartet structure is not observed due to the remarkable width of the lines. Moreover, the relative splittings cannot be reproduced by Ham's theory of spin-orbit quenching[3] and the relative intensities are different from those predicted by crystal-field theory. As regards MgO:V the experimental characteristics of the ZPL have recently been explained by taking into account the intensity quenching operated by the Jahn-Teller effect[1] (JTE) and the existence of fast nonradiative transitions from $^4T_2$ to the ^2E and $^2T_1$ states.[4,5] Such nonradiative transitions are induced by the spin-orbit interaction which mixes the discrete zero-phonon states of $^4T_2$ with the vibrational continua relative to the underlying doublets ^2E and $^2T_1$. As shown in Refs. 4 and 5, the nonradiative transition probability is proportional to the squared spin-orbit coupling parameter ζ^2 and to the vibrational overlap integral $G(\omega)$.

The experimental situation is less favorable in MgO:Cr because the ZPL is superimposed on the odd-phonon-induced sideband relative to $^2T_1$ which has electric dipole character;[2] moreover, the spin-orbit components of the ZPL are broader and the respective energies, intensities, and widths have not been well determined so far.[2,6] The observed larger widths have been partially accounted for in Ref. 5 by considering that both ζ and $G(\omega)$ are larger for MgO:Cr than are for MgO:V. However, the JTE on $^4T_2$ was not taken into account because its strength was not known.

In this paper we will present Zeeman measurements on MgO:Cr and we will show that by means of this technique it is possible to individuate, to a reasonable extent of reliability, the different components of the ZPL. In this way it will become possible to apply the theoretical methods of Refs. 4 and 5 to MgO:Cr by including the JTE. The agreement between theory and experiment, though quite satisfactory, is in this case less quantitative than for MgO:V, owing to objective experimental difficulties and to partial breakdown of the assumptions on which the theoretical treatment of Refs. 4 and 5 is based. It should be noted, however, that carrying out a more accurate calculation appears to be extremely difficult. It should also be mentioned that similar experiments on MgO:Cr have been recently reported by Pörsch and Manson[6]; their data are, however, less complete than ours, and their assignment of the experimental peaks to the spin-orbit substates appears to be partially incorrect.

II. EXPERIMENTAL

A. Apparatus and results

The MgO:Cr sample (1300 ppm nominal concentration, cut along the ⟨100⟩ directions) was placed in the bore of a superconducting magnet and immersed in pumped liquid helium at 1.7 K. At this temperature and with a field of 54 kG, only the $m_s=-\frac{3}{2}$ substate of the $^4A_2$ ground state ($g=1.98$) is appreciably populated. The cubic centers were isolated by recording the excitation spectrum of the R line at 14 325 cm^{-1}, as described in Ref. 7.

The dichroism effect was revealed both by lock-in detection, by means of a low-frequency rotating quarter-wave plate, and by detecting the spectra in different circular polarizations by a photon-counting plus multichannel system. The latter method is much less noisy than the former, and in the following we will report only the multichannel spectra. On the other hand, the difference of the α^+ and α^- multichannel spectra was compared to the magnetic circular dichroic (MCD) spectrum of the lock-in, in order to make sure that the α^+ and α^- spectra (which were taken at different times) were free from spurious differences due to long-range fluctuations of the apparatus.

The zero-field excitation spectrum at 8 K has been reported elsewhere [Fig. 1(a) of Ref. 2] and it shows, in order of increasing energy, the sideband relative to ^2E, the two sharp lines at about 15 000 cm^{-1} corresponding to the Γ_8 and Γ_6 zero-phonon components of $^2T_1$, and the much stronger structure of $^4T_2$ ZPL. The emission sideband relative to ^2E, and the calculated sideband relative to $^2T_1$ are also reported in Ref. 2; it is shown there that some of the weaker structures near the $^4T_2$ ZPL are actually due to this sideband. If one is interested in the form of the $^4T_2$ ZPL, such a sideband must be subtracted.

The experimental spectra under magnetic field and with different polarizations are reported in Figs. 1(a)—1(d); the different polarizations are labeled as in Manson and Sturge's paper.[8] Since all of these spectra are excitation spectra, their intensities are arbitrary; in particular, the σ and π spectra (light incident perpendicular to the static magnetic field H_0) were taken with a different experimental geometry with respect to α^+ and α^- (light incident parallel to H_0). Since, as we shall see in the following, we will have to compare spectra taken with different geometries, we must eliminate such scale-arbitrariness as far as possible. This was done by normalizing each magnetic-field spectrum to the corresponding zero-field one. In the case of α^+ and α^- the error introduced by this procedure is estimated to be about 2%, whereas for σ and π we expect about 5%; this larger error is caused by the different response, in these two polarizations, of the excitation monochromator, so that a further correction for this effect was necessary. The energy resolution is set by the Jobin-Yvon excitation monochromator to ~ 5 cm^{-1} in the range of interest.

As regards the polarization efficiency, the upper limit of all kinds of inefficiencies is given by the

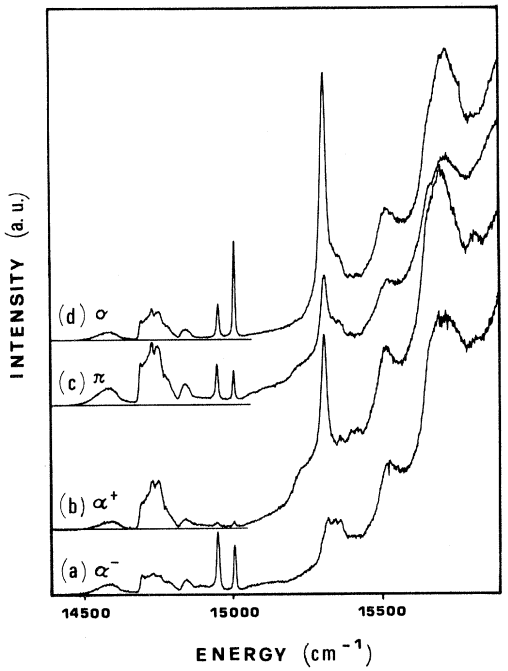

FIG. 1. Excitation spectra under magnetic field (54 kG), $T=1.7$ K, in different polarizations. Resolution 5 cm^{-1}.

intensity of the $^2T_1$ ZPL's in α^+, because they should be absent in this polarization. What we find is that $I(^2T_1,\alpha^+) \sim 5\%[I(^2T_1,\alpha^-)]$.

B. Analysis of the data

The $\alpha^+-\alpha^-$ spectrum, obtained by subtracting the spectra of Figs. 1(a) and 1(b), and which is equivalent to the MCD spectrum, is shown in Fig. 2(a). By comparing our data with those of Pörsch and Manson[6] we note that, as regards the ZPL of $^4T_2$, the $\alpha^+-\alpha^-$ spectra are practically the same, whereas the separate α^+ and α^- spectra of the present paper are appreciably different from theirs. These differences will be discussed in the following.

Since in the spectral range of interest, absorption is due to both magnetic dipole transitions and to vibration-induced electric dipole transitions,[1] it is of interest to separate the two kinds of contributions. The structures due to magnetic dipole transitions are the only ones left after the σ spectrum is subtracted from the $(\alpha^++\alpha^-)/2$ one. In fact, for an electric dipole transition the σ spectrum is equivalent to $\alpha^++\alpha^-$, because the only difference between the two is the direction of the incident light with respect to the static field, while the elec-

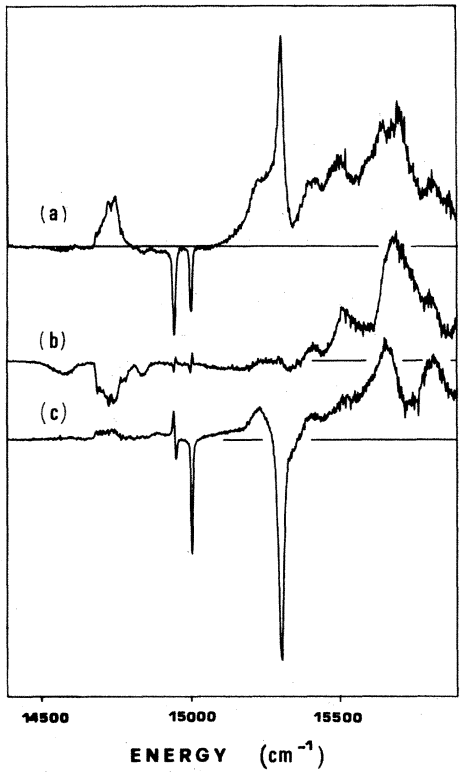

FIG. 2. (a): $\alpha^+-\alpha^-$, (b): $(\alpha^+ +\alpha^-)/2-\pi$, (c): $(\alpha^+ +\alpha^-)/2-\sigma$. The reported combinations of spectra are obtained from the spectra of Fig. 1.

tric field of light is in both cases perpendicular to the static field. Thus, by subtracting σ from $(\alpha^+ +\alpha^-)/2$ the electric dipole contribution cancels out. The opposite (i.e., cancellation of the magnetic dipole structure) happens by subtracting π from $(\alpha^+ +\alpha^-)/2$.

Such spectra combinations are reported in Figs. 2(b) and 2(c). As expected, all of the zero-phonon structures turn out to have magnetic dipole character, while the sideband of ^2E is mainly due to electric dipole transitions. The weak electric dipole signal in Fig. 2(b) at the energy of the $^4T_2$ ZPL may be interpreted as due to the sideband of $^2T_1$, its shape being in agreement with the computed sideband (see the next section). The weak resonance corresponding to the $^2T_1$ ZPL's is spurious in Fig. 2(b) and is due to a very small relative shift between the experimental spectra whose subtraction gives this figure and which is important only for the sharpest features. On the other hand, the resonance corresponding to $\Gamma_8(^2T_1)$ in Fig. 2(c) is not spurious but is due to Zeeman splitting of this level. It should also be noted that the sideband relative to $^4T_2$ has both electric and magnetic dipole character, and that the two contributions are of the same order of magnitude as expected, since a similar behavior is observed in the $^2E \leftrightarrow {}^4A_2$ transition.[2] It is also interesting to note that the shape of the electric dipole contribution to this latter sideband very closely resembles the shape of the ^2E sideband, whereas the magnetic dipole part is rather different, and its peak energies almost coincide with the Raman peaks computed by Billat[9] at ~ 380 cm^{-1} (ϵ_g phonons) and at ~ 570 cm^{-1} (α_{1g} phonons). Since the relative intensities are comparable, the coupling strength to phonons of both symmetries must be of the same order of magnitude.

III. DISCUSSION

The zero-phonon $^4A_2$-$^2T_1$ transition is partially allowed by spin-orbit mixing between the $^2T_1$ and $^4T_2$ states; a perturbative calculation predicts that the transitons to the Γ_6 and Γ_8 sublevels will have the same intensity without magnetic field. The observed ratio $I(\Gamma_6)/I(\Gamma_8)=1.4$ is slightly different from unity. This is not surprising because these states are placed near in energy to the $^4T_2$ absorption band, which in a perturbative (or crystal-field) calculation is treated as one discrete level, without taking into account the electron-phonon interaction. As regards the calculated intensities under magnetic field, in the various polarizations and for very low temperature, they are reported in Table I. These intensities are relative to the respective in-

TABLE I. Calculated magnetic dipole intensities under magnetic field in different polarizations. Initial state: $^4A_2(m_s=-\frac{3}{2})$. The intensities are relative to the respective intensities without magnetic field.

		α^+	α^-	σ	π
$^2T_1$	Γ_8	0	2	1	1
	Γ_6	0	1	2	$\frac{1}{2}$
$^4T_2$	Γ_7	3	0	0	$\frac{3}{2}$
	Γ_8	$\frac{6}{5}$	0	$\frac{9}{5}$	$\frac{3}{5}$
	Γ_8'	$\frac{3}{10}$	$\frac{5}{2}$	$\frac{1}{5}$	$\frac{14}{10}$
	Γ_6	0	1	2	$\frac{1}{2}$

tensities without magnetic field. (See Fig. 7.) The observed intensities agree with the computed ones within 5%. The presence in α^+ [see Fig. 1(b)] of weak signals due to Γ_6 and Γ_8 may be spurious, as discussed in the preceding section.

Following the procedure of Ref. 2, the structures superimposed on the $^4T_2$ ZPL which are due to odd phonons relative to $^2T_1$ can be subtracted. The basic assumption that we make in order to compute the $^2T_1$ sideband is that the mechanism which gives rise to it is the same as for the ^2E sideband: spin-orbit mixing between $^2T_1$ and $^4T_2$, plus mixing of $^4T_2$ into higher-lying odd electronic states, operated by T_{1u} and T_{2u} phonons. On the basis of this assumption Manson and Shah,[10] from MCD measurements on the ^2E-$^4A_2$ emission, obtained the densities of states and the coupling strengths for T_{1u} and T_{2u} vibrations. By applying the calculation method of Ref. 10 to the absorption transitions $^4A_2$-^2E and $^4A_2$-$^2T_1$ we obtained for the various polarizations the transition probabilities reported in Table II, where, again, the transition probabilities are relative to the zero-field ones.

If we indicate by $F_{1u}(\omega)$ and $F_{2u}(\omega)$ the contributions from T_{1u} and T_{2u} phonons, respectively, to the sideband relative to ^2E, $I(\omega)$, from Table I we have (i) without field,

$$I(\omega)=F_{1u}(\omega)+F_{2u}(\omega)\ , \tag{1}$$

(ii) with field and at low temperature ($m_s=-\frac{3}{2}$ of $^4A_2$ is the only populated state)

$$I(\alpha^+)=\tfrac{3}{8}F_{1u}(\omega)+\tfrac{9}{8}F_{2u}(\omega)\ , \tag{2}$$

$$I(\alpha^-)=\tfrac{9}{8}F_{1u}(\omega)+\tfrac{3}{8}F_{2u}(\omega)\ , \tag{3}$$

$$I(\pi)=\tfrac{12}{8}F_{1u}(\omega)+\tfrac{12}{8}F_{2u}(\omega)\ , \tag{4}$$

$$I(\sigma)=\tfrac{6}{8}F_{1u}(\omega)+\tfrac{6}{8}F_{2u}(\omega)\ . \tag{5}$$

F_{1u} and F_{2u} may be obtained by inverting Eqs. (2) and (3) and are shown in Fig. 3; the remaining three equations have been used to check the intensities but not the shapes, because in these equations F_{1u} and F_{2u} have the same coefficients. Actually, as is seen from Figs. 1(c) and 1(d) and from the zero-field spectrum reported in Ref. 2, the shape of the sideband does not change, and the intensity ratios agree with the ones computed with Eqs. (1), (4), and (5). As already observed in emission,[10] the coupling to T_{2u} modes is stronger; also, the emission and absorption computed band shapes are very similar but not identical to each other. This difference is reflected by the change of sign in the MCD spectra in the low-energy side (acoustical phonon) and in the small structure at high energy (about 550 cm^{-1} from the zero-phonon line). This difference cannot be explained at present, because even the inclusion of α_{1g} and ϵ_g phonons does not change the sign of the MCD spectrum in passing from absorption to emission. Detailed calculations show that phonons of any symmetry give the same MCD spectra in emission and in absorption, the only difference between the two being that the MCD signal in absorption is 3 times more intense than in emission.[11] The observed difference in MgO:Cr is quite small and is only visible in the dichroic spectra, unlike the case of ruby where the difference is much stronger.[12]

By using Table II it is now possible to determine the shape of the sideband relative to $^2T_1$ for all polarizations. We assume that in absence of magnetic field the shape of the sideband relative to $\Gamma_8(^2T_1)$ and to $\Gamma_6(^2T_1)$ is the same as that of ^2E, with an intensity which is proportional to the intensity of the respective ZPL's in absorption. Such relative intensities have been determined by the excitation spectrum of the ^2E sideband, which also shows the R line.

In a generic polarization P we have for the band shape

TABLE II. Calculated electric dipole transitions induced by T_{1u} and T_{2u} odd phonons. Initial state: $^4A_2$ ($m_s=-\frac{3}{2}$). The intensities are relative to the respective intensities without magnetic field.

		T_{1u}				T_{2u}			
		α^+	α^-	σ	π	α^+	α^-	σ	π
^2E	Γ_8	$\frac{3}{8}$	$\frac{9}{8}$	$\frac{6}{8}$	$\frac{12}{8}$	$\frac{9}{8}$	$\frac{3}{8}$	$\frac{6}{8}$	$\frac{12}{8}$
$^2T_1$	Γ_8	$\frac{1}{2}$	$\frac{3}{2}$	1	1	$\frac{3}{2}$	$\frac{1}{2}$	1	1
	Γ_6	1	$\frac{3}{2}$	$\frac{5}{4}$	$\frac{1}{2}$	$\frac{3}{2}$	1	$\frac{5}{4}$	$\frac{1}{2}$

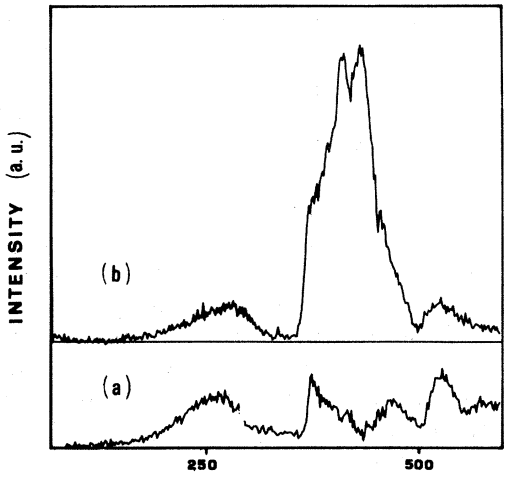

FIG. 3. Computed (see text) contributions to the sideband relative to ^2E from phonons of (a) T_{1u}, and (b) T_{2u} symmetry.

$$B^P(E)=\sum_{i=1,2}\sum_{\gamma=6,8}\frac{I(\Gamma_\gamma,{}^2T_1)}{I({}^2E)}A^\gamma_{T_{1u}}(\Gamma_\gamma,{}^2T_1)\times F_{iu}[\hbar\omega=E-E(\Gamma_\gamma,{}^2T_1)]\ , \tag{6}$$

where the I's are the experimental intensities of the ZPL's without field, $\Gamma_\gamma=\Gamma_8,\Gamma_6$, $i=1,2$ labels the odd irreducible representations, and the A's are the computed coefficients as reported in Table II.

The sidebands obtained by Eq. (6) are reported in Figs. 4(c), 5(c), and 6(c) for the three independent polarizations α^+, α^-, and π, respectively. In the same figures [part (a)] the experimental spectra from which the sidebands have been subtracted are reported. The scales of Figs. 4–6 are different from each other. By comparing these spectra to those of Fig. 1, we note that some of the structures which are observed in the spectral range of the $^4T_2$ ZPL disappear in the subtracted spectra. This is satisfying even though the sidebands have been computed under some restrictive assumptions. For instance, in the case of MgO:V, where the $^2T_1$ sideband is directly observed, it was found that the method used here yields the correct band shape but not the correct intensity.[1] This was ascribed to different coupling mechanisms which have not been included here. Because of these reasons, it is clear that the results of our subtraction procedure are not exact, but in any case better than no subtraction at all.

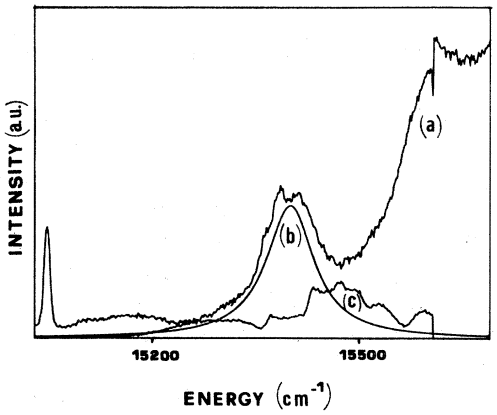

FIG. 5. Same as Fig. 4, but for α^-.

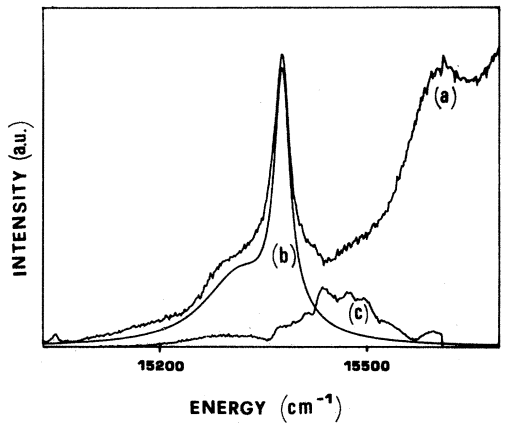

FIG. 4. (a) Experimental α^+ spectrum, to which the computed sideband relative to $^2T_1$ [shown in (c)] has been subtracted; (b) Lorentzian fit with the parameters reported in Tables II and III.

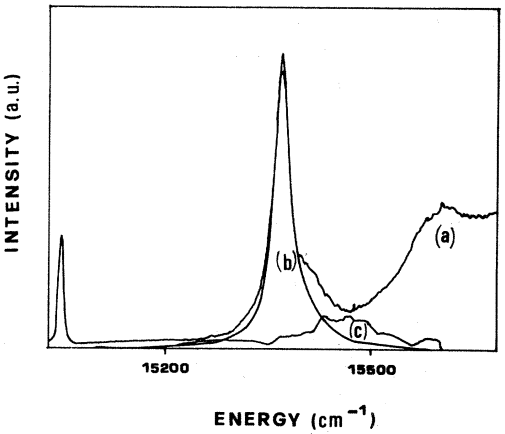

FIG. 6. Same as Fig. 4, but for σ.

We now turn to the $^4T_2$ ZPL, which should, in principle, show a quartet structure. The computed transition probabilities to the various spin-orbit sublevels ($\Gamma_7, \Gamma_8, \Gamma_6, \Gamma_8'$) in the different polarizations are summarized in Table I. This table is to be read in the following way: Assume that $I_0(\Gamma)$ is the intensity of the Γ component of the ZPL without magnetic field; the intensity $I^P(\Gamma)$ under magnetic field and in the P polarization is given by I_0 times the corresponding factor in Table I. It should be noted that I_0 may be different from the intensity one expects on the basis of crystal-field theory [which predicts $I(\Gamma_8)=I(\Gamma_8')=2I(\Gamma_7)=2I(\Gamma_6)$], because of the selective intensity quenching operated by the dynamical JTE,[13] which may reduce the intensity of the higher-energy lines (Γ_8' and Γ_6) by a factor ~ 2. Therefore, not only the energies and widths of the lines but their intensities as well must be determined by the experimental data.

From Figs. 4–6 and from Table I, it is evident that the sharpest and most intense peak belongs to Γ_8 because it is very intense in σ, intense in α^+, and it disappears in α^-. The broad shoulder on the low-energy side of Γ_8, which is only present in α^+, is to be attributed to Γ_7. As regards Γ_6 and Γ_8', since they never appear separately from each other (except in α^+ where, however, Γ_8' is expected to be very weak), the situation is less clear. However, from Table I we expect that in α^- in practice only Γ_8' is present, whereas in σ the shoulder on the high-energy side of Γ_8 should correspond to Γ_6.

In order to get more quantitative information from the spectra, we have made the following assumptions:

(i) The zero-field mixing between Γ_8 and Γ_8' has been neglected.

(ii) The mixing of the levels induced by the static magnetic field has been neglected.

(iii) All lines have been assumed to have a Lorentzian shape.

Hypothesis (i) is based on the expected mutual cancellation of second-order spin-orbit and Jahn-Teller induced mixings in analogy to the MgO:V case,[1,8] and it is legitimized by the total absence of Γ_8 in α^-. Neglect of magnetic-field-induced mixing [hypothesis (ii)], which corresponds to the assumption that the only effect of the magnetic field is to populate selectively the sublevels of $^4A_2$, is justified by the smallness of the Zeeman Hamiltonian with respect to the spin-orbit Hamiltonian and to the widths of the levels. In this regard, we have verified that the polarized spectra did not change appreciably by varying the static field from 54 to 20 kG, at which field value the population of the $m_s=-\frac{1}{2}$ sublevel of $^4A_2$ becomes appreciable. As regards hypothesis (iii) (Lorentzian shape), this means that the broadening of the lines is mostly homogeneous. This is jutified by the existence of very fast nonradiative transitions from $^4T_2$ to $^2T_1$ and to ^2E; moreover, the strain-induced broadening of the lines seems to be negligible. In fact, measurements on samples with different Cr concentration, while showing changes of almost 1 order of magnitude in the width of the sharp R emission, left the shape and width of the $^4T_2$ ZPL unchanged. It should be noted, however, that even if the broadening is homogeneous, this does not ensure that the shape is Lorentzian, especially for the broader lines like $\Gamma_7(\Delta E \sim 120\ \mathrm{cm}^{-1})$ because this happens only if the density of vibrational states of the interacting continuum is nearly constant over a range $\sim \Delta E$.[5] However, in order to keep our analysis as simple as possible, we have fitted the spectra with Lorentzian curves.

The best fit to the four spectra of Figs. 4–7, by keeping the intensity ratio of each line in the various spectra fixed to the values given in Table I, is given by the widths, intensities, and peak energies summarized in Table III. The line shapes resulting from summing up the respective Lorentzians are

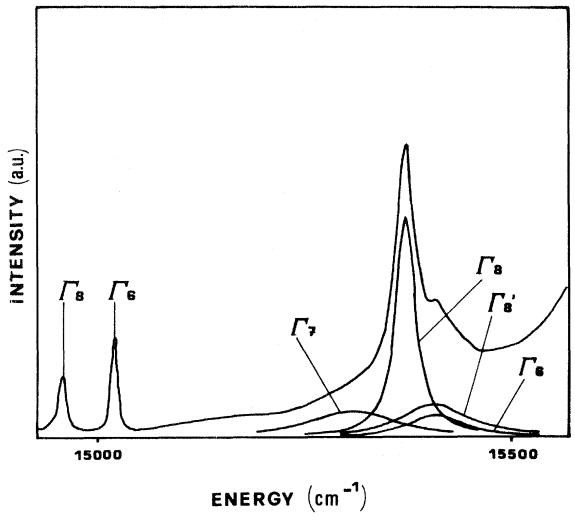

FIG. 7. Zero-field excitation spectrum to which the $^2T_1$ sideband has been subtracted: The single Lorentzians which give the best fit to $^4T_2$ ZPL are reported and labeled. The components of $^2T_1$ ZPL are also labeled.

TABLE III. Experimental intensities, widths, and energies of the $^4T_2$ zero-phonon line components. Intensities and energies are relative to Γ_8.

	Γ_7	Γ_8	Γ_8'	Γ_6
Relative intensity	0.52±0.05	1	0.5±0.1	0.26±0.05
Width (cm^{-1})	120±20	26.5±0.5	90±20	70±20
Relative energy (cm^{-1})	−60±10	0	25±10	25±20

shown by curves (b) of Figs. 4–6. As it results from the spectra, the quantities relative to Γ_8 are the less affected by uncertainty, and for this reason the energy positions and intensities of Table III have been normalized to Γ_8's. The peak energies of Table III refer to the zero-field spectrum; actually, in the different polarizations, shifts due to the magnetic field are observed, but they are too small with respect to the widths to yield reliable values of the g factors. The main cause of uncertainty, especially for Γ_6 and Γ_8', is the presence of a rather intense background due to the sideband's tail. As regards Fig. 5, the origin of the weak structures superimposed on Γ_8' is obscure. Neither of the weak structures on the top of Γ_8' corresponds to Γ_8 so that they cannot be attributed to spurious effects due to inefficient polarization. An explanation could be found in the possibility of non-Lorentzian line shapes for Γ_8 and Γ_8', as discussed above since $E(\Gamma_8',\Gamma_6)-E(^2T_1,\mathrm{ZPL})\sim\hbar\omega_{\mathrm{vib}}$.

It is interesting now to examine in detail the differences between our results and those of Ref. 6 and the relative assignments of the observed structures. In Ref. 6 the main structure (corresponding to Γ_8) is present, though less intense, in α^- as well; as a consequence those authors attributed this structure to the three degenerate levels Γ_7, Γ_8, and Γ_6. However, from our α^+ spectrum it is evident that Γ_7 gives rise to a well-separated structure at lower energy. As regards the presence of the main structure in α^- in Ref. 6, this is probably due to a temperature effect. In fact, the selection rules of Table I are based on the assumption that only $m_s=-\frac{3}{2}$ ($^4A_2$) is populated; in our experimental conditions ($H_0=54$ kG, $T=1.7$ K) this requirement is fulfilled, whereas in the case of Ref. 6 ($H_0=50$ kG, $T=5$ K) about 20% of the population is absent from the lowest state.

The most interesting result of our analysis is the singling out of Γ_7, which appears to be unusually broad and shifted to low energy. This structure, well evident in α^+, is only a weak shoulder in the zero-field spectrum (see Fig. 7), and was previously attributed to the acoustic branch of the phonon sideband relative to $^2T_1$.[2] From the intensity data reported in Table III, it is clear that the intensity quenching operated by the Jahn-Teller effect[13] is severe, because the observed intensities of Γ_8' and Γ_6 are reduced by about a factor of 2 with respect to what was expected from crystal-field predictions. This indicates a rather strong Jahn-Teller effect but does not allow its quantitative evaluation because the quenching effect depends strongly on the density of the interacting vibrational states.[13] We also note that from our data, the Γ_8-Γ_8' splitting (~ 25 cm^{-1}) results to be lower than the one previously deduced from stress[2] and MCD (Ref. 6) data [40–50 cm^{-1}, see also Fig. 2(a)]. The present interpretation is in agreement with the stress data as regards Γ_8 and Γ_8'; it is still to be fully understood why the Γ_7 state, which is easily observed in the present measurements, should not be observed in the stress-induced linear dichroism spectra.[2]

IV. VIBRONIC COUPLING AND NONRADIATIVE TRANSITIONS

On the basis of the present experimental data, previous interpretation[2,14] of the shape of the $^4T_2$ ZPL must be reconsidered. In the case of V^{2+} impurities in MgO (Refs. 1 and 4) and $KMgF_3$ (Ref. 13), the shape of such ZPL has been satisfactorily interpreted by taking into account the selective intensity quenching caused by the JTE,[13] and the effect of nonradiative transitions from $^4T_2$ to the doublet states ^2E and $^2T_1$.[4] In particular, the computed broadening and shifts of the lines could well account for the experimental line shape. This was

possible because the JTE in MgO:V is weak enough as to be satisfactorily treated by perturbation theory.

The situation is much more complicated in MgO:Cr because, on one hand the JTE is stronger and not easily evaluated, and on the other hand the spin-orbit coupling is also stronger, which implies that all broadening and shifting effects are more pronounced. Finally, the energy gaps, and especially that between $^2T_1$ and $^4T_2$, are smaller.

The strength of the JTE is, in general, deduced by the quenching of the crystal-field spin-orbit splitting [the unquenched overall splitting should be ~ 150 cm^{-1} in this case, with a coupling constant $\zeta = 225$ cm^{-1} (Ref. 15)], but this is not possible in MgO:Cr because other effects (i.e., second-order spin-orbit coupling which causes a Lamb shift) are more important. In fact, in the absence of Lamb shift one expects $E(\Gamma_6)=E(\Gamma_8')$ and

$$[E(\Gamma_8)-E(\Gamma_7)]/[E(\Gamma_8')-E(\Gamma_8)]=0.6 .$$

On the contrary, as seen from Table III, this ratio is actually ~ 2. As a consequence, the Ham quenching factor deduced from the experimental splittings varies from ~ 0.2 to ~ 1, according to the pair of levels one considers. In this situation we will see, however, that an estimate of the strength of the JTE can be obtained by the width of Γ_7 relative to Γ_8's.

A quantitative evaluation of the values of the Lamb shifts is even less reliable. This can be understood by inspection of Fig. 8 where we have schematically drawn the $^4T_2$ ZPL and the densities of vibrational states, relative to ^2E and to $^2T_1$, as "seen" by this ZPL. Since the shift is due to second-order spin-orbit interaction between the ZPL and these densities of states, it is clear that while $^2T_1$ pushes towards low energy, the sign of the displacement due to ^2E is practically unknown; moreover, the various spin-orbit sublevels of the ZPL are shifted by different amounts, strongly dependent on the coupling to Jahn-Teller modes.

Roughly speaking, since both broadening and shift increase with increasing the discrete-continuum interaction, we expect the broader levels to be the more shifted. If for each level the resulting shift is to low energy (see Fig. 8), it is to be expected that Γ_7 moves away from Γ_8 while Γ_8' and Γ_6 get nearer to it, in qualitative agreement with what is observed.

More quantitatively, it was shown in Ref. 5 that the order of magnitude of the broadening of the levels (apart from Γ_7) can be obtained by a simplified model which neglects the JTE. The results of such a calculation are reported in Table IV, where the contributions due to ^2E and $^2T_1$ are shown separately. The calculation is based on the same assumption as reported in Ref. 5, Sec. III; the den-

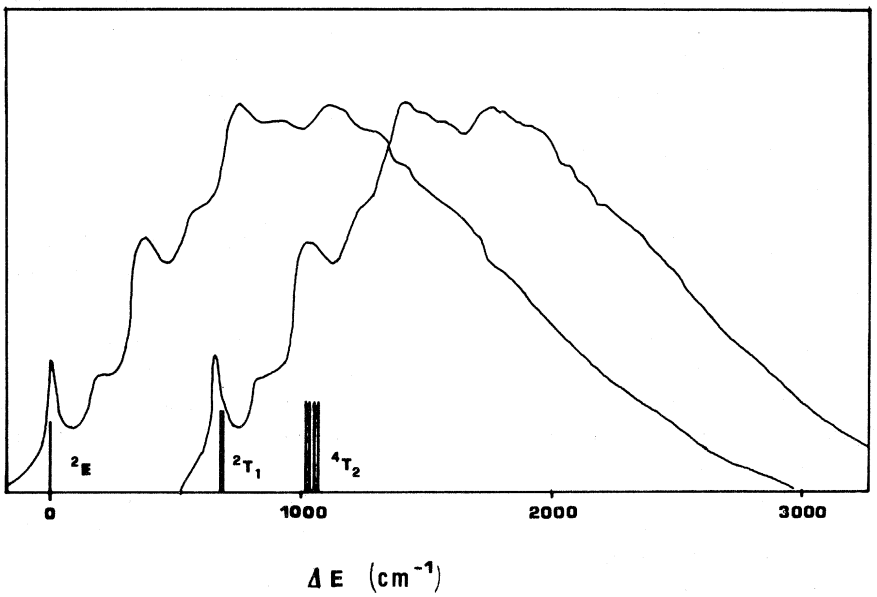

FIG. 8. Schematic energy-level diagram showing the $^4T_2$ zero-phonon line and the sidebands relative to ^2E and $^2T_1$. The zero-phonon line relative to these latter levels are also reported.

sity of states $G(\omega)$ has been computed by assuming a pekarian absorption band shape with parameters

$$\hbar\omega_1 = 500\ \text{cm}^{-1},\quad S = 2.2\ ,$$

S being the Huang-Rhys factor and ω_1 the effective vibrational frequency of totally symmetrical modes. It should be noted that as regards ^2E, the value of $G(\omega)$ that we need[5] is very near to the band maximum, and therefore its estimate is quite reliable and not very dependent on the parameter's values; in contrast, for $^2T_1$ $G(\omega)$ must be calculated in the low-energy part of the spectrum, where phonon structures are to be expected. The computed value is therefore less reliable, and the resulting shape of the broadened line could even be non-Lorentzian. In any case, it follows from Table IV that the states are mainly broadened by the interaction with ^2E, except for Γ_6 which only couples to $^2T_1$.

At this stage of approximation (no JTE) Γ_7 is not broadened because the electronic states ^2E and $^2T_1$ do not contain the irreducible representation Γ_7.[5] Inclusion of the JTE mixes the electronic state of $^4T_2$, in this way allowing nonradiative transitions from all the sublevels of the ZPL. This redistribution of width is strongly affected by interference phenomena among the wave functions, and as such it is very dependent on the strength of the JTE. If the latter were very strong, one would expect all the lines to be more or less equally broadened. The average width in this case would be $\sim 100\ \text{cm}^{-1}$, as results from Table IV by taking into account the level's degeneracy. The average experimental width is, from Table III, $\sim 70\ \text{cm}^{-1}$, which compares reasonably well with the computed value.

To get an idea of what happens with intermediate JTE, we can apply the perturbative treatment of Ref. 5, which still gives reliable results for the interaction between $^4T_2$ and ^2E. In Fig. 9 we report the widths of the components of the $^4T_2$ ZPL as a function of the Jahn-Teller coupling to ϵ_g modes, and assuming an effective phonon energy $\hbar\omega_\epsilon = 330\ \text{cm}^{-1}$. It is seen that by increasing the Jahn-Teller coupling a redistribution of widths takes place which involves mainly Γ_7 and Γ_8'. Since this model assumes only one Jahn-Teller active frequency, allowing only α_{1g} modes to have a continuum of frequencies, it can be used only for small values of the Jahn-Teller coupling, which is measured by the Jahn-Teller energy E_{JT}. Since the JTE is treated perturbatively, it is necessary that the coupling to α_{1g} modes be much stronger than to ϵ_g modes. This is the case of MgO:V, and the results of the calculation are in excellent agreement with experiment in this system.[5] In the present case, however, where the two couplings are comparable in strength, only qualitative information can be obtained. In fact, from the calculation it appears that in order to get $\Delta E(\Gamma_7) \sim 100\ \text{cm}^{-1}$ (as observed experimentally), it would be necessary to consider Jahn-Teller couplings that are so strong as not to be treated perturbatively.

In any case it is interesting to note that the width exchange involves in practice only Γ_8' and Γ_7, leaving Γ_8 and Γ_6 practically unchanged. In this way the unexpectedly large width of Γ_7 (which

TABLE IV. Computed widths of the $^4T_2$ zero-phonon line components without taking into account the Jahn-Teller effect. The contributions due to nonradiative transitions to the levels reported in the first column are shown.

		Γ_7	Γ_8	Γ_8'	Γ_6
^2E	Γ_8	0	22	200	0
$^2T_1$	Γ_8	0	7	30	0
	Γ_6	0	0	0	71
Total		0	29	230	71

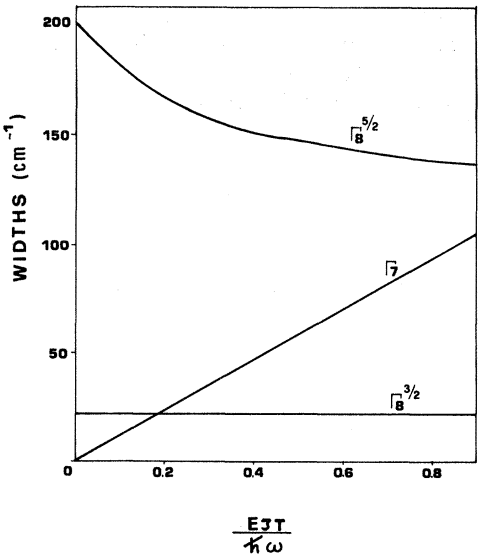

FIG. 9. Computed widths of the $^4T_2$ zero-phonon line components, as a function of the Jahn-Teller coupling to ϵ_g modes. Only the interaction with the ^2E continuum has been considered (see text).

should be zero without JTE) can be understood because, as seen from Fig. 9, even for moderate values of E_{JT} Γ_7 is broader than Γ_8. This effect, which has already been observed in MgO:V,[1,5] is due to interference between the spin-orbit and Jahn-Teller interactions; such interference is constructive for Γ_7 and destructive for Γ_8.

As regards the splittings of the levels, this method does not yield reliable values, since they are very dependent on the parameters' values (E_{JT},$\hbar\omega_\epsilon$,S,$\hbar\omega_1$); the computed values, however, are in qualitative agreement with the previous discussion on the low-energy displacement of the levels. In any case, the experimental data on the widths indicate the presence of a rather strong JTE, which implies a strong quenching of the first-order spin-orbit interaction. This indicates that the observed splitting are mostly due to the Lamb shift, consistent with the rather odd splitting pattern that cannot be reproduced by the usual Ham quenching theory.

A more accurate calculation would require the JTE to be taken into account more properly by allowing the frequency of Jahn-Teller active modes to vary continuously.

ACKNOWLEDGMENTS

The authors wish to thank Professor E. Duval and Dr. A. Boyrivent for useful discussions. This work was partially supported by the Consiglio Nazionale delle Ricerche (CNR), Contract No. 80.02409.02.

[1]G. Viliani, O. Pilla, M. Montagna, and A. Boyrivent, Phys. Rev. B 23, 18 (1981), and references therein.
[2]A. Boyrivent, E. Duval, M. Montagna, G. Viliani, and O. Pilla, J. Phys. C 12, L 803 (1979), and references therein; A. Boyrivent and E. Duval, *ibid.* 11, L227 (1978).
[3]F. S. Ham, Phys. Rev. 138, A1727 (1965).
[4]M. Montagna, O. Pilla, and G. Viliani, Phys. Rev. Lett. 45, 1008 (1980).
[5]O. Pilla, M. Montagna, and G. Viliani, Phys. Rev. B 24, 666 (1981).
[6]J. Pörsch and N. B. Manson, Phys. Status Solidi B 104, K7 (1981).
[7]O. Pilla, M. Montagna, G. Viliani, and S. Santucci, Phys. Rev. B 21, 4859 (1980).
[8]N. B. Manson and M. D. Sturge, Phys. Rev. B 22, 2861 (1980).
[9]A. Billat, thesis, Université de Reims, 1978 (unpublished); A. Billat, J. P. Mon, and M. Voisin, J. Phys. C 9, 1337 (1976).
[10]N. B. Manson and G. A. Shah, J. Phys. C 10, 1991 (1977).
[11]M. Ferrari, thesis, Università di Trento, 1981 (unpublished).
[12]D. F. Nelson and M. D. Sturge, Phys. Rev. 137, A1117 (1965).
[13]M. Montagna, O. Pilla, and G. Viliani, J. Phys. C 12, L699 (1979).
[14]R. Lacroix, J. Weber, E. Duval, and A. Boyrivent, J. Phys. C 13, L781 (1980).
[15]W. A. Runciman and K. A. Schroeder, Proc. R. Soc. London, Ser. A 265, 489 (1962).